Packaging of PIN Photodiode on Patch Antenna for a Dual-Mode Indoor RF/FSO Receiver

Jun Liao, Ali Mirvakili, Anatoliy O. Boryssenko, *Member, IEEE*, Valencia M. Joyner, *Member, IEEE*, and Zhaoran Rena Huang, *Member, IEEE*

***Abstract*—This paper reports the design, packaging and characterization of a miniaturized dual-mode radio-frequency (RF)/free space optical (FSO) indoor wireless receiver module. Two different patch antennas are designed and integrated with bare die photodiodes together with transimpedance amplifier (TIA) circuits on a printed circuit board (PCB). Ansoft HFSS is used to predict the coupling from RF to FSO link. Measurement results verify that optical link degradation is minimized with the specially designed patch structure. FSO link operation at 2 Gb/s in a 10 GHz RF environment is achieved. Through the comparison to previously developed RF/FSO modules, the new receiver boards demonstrate reduced RF-to-optical cross channel coupling, and increased gain and antenna radiation efficiency.**

***Index Terms*—Dual mode wireless communication, free space optics, hybrid packaging, patch antenna.**

I. Introduction

With the rapid development of information technology, there is an increasing demand for high-speed ubiquitous wireless networks. The traditional radio-frequency (RF) communication system has limitations on speed, security, and power consumption. In recent years, free space optical (FSO) communication, which demonstrates high data transmission bandwidth, low-power consumption, and high security, has drawn considerable research interest [1]. However, the application of FSO communication is challenged by the optical line-of-sight alignment issue. A FSO data transmission system with RF channels as the backup was proposed as a viable system architecture to improve wireless network reliability. The software-level algorithms to support routing and coding of the RF/FSO hybrid network has been investigated in previous work [2]–[4]. As for RF/FSO system hardware development, assembly of discrete components, monolithic integration, and hybrid packaging are the major packaging approaches at present [5]–[7]. These system demonstrations focus on the RF and optical components separately requiring large surface area compared to an integrated approach.

It is of great interest to develop miniaturized RF/FSO transceiver packages for many emerging applications, especially for high speed indoor wireless access. In a typical indoor environment, the loss of optical signal due to atmosphere attenuation is negligible, and therefore there is no optical amplifier (no gain) required for the receiver in such a short range. In previous papers, the authors proposed and demonstrated a new kind of hybrid packaging scheme where the RF antenna and the optical elements share the common metal pads [8]–[10]. The metal pads are placed in the vicinity of the antenna to direct the RF channel radiation, as well as provide electrical connections for the optical devices. However, the modified quasi-Yagi antenna has only 0.5 dBi gain perpendicular to the antenna substrate, and the coupling from antenna to PIN receiver is not negligible.

To overcome the abovementioned drawbacks of the RF/FSO module developed in previous works, in this research, we explore new antenna schemes with high gain perpendicular to printed circuit board (PCB), and optimize the package structure to achieve minimized inter-channel coupling. Modified microstrip patch antennas on both low and high dielectric substrates are studied extensively in this paper to replace the modified quasi-Yagi antenna in previous publications. As discussed later in this paper, the antenna gain is significantly improved in normal direction, and an optimized package layout is achieved with patch antenna for minimized coupling.

Patch antenna is a planar antenna that is compatible with monolithic microwave integrated circuit (MMIC) technology. It offers a number of advantages compared to the quasi-Yagi antenna based RF/FSO package. First, there is less performance degradation for the patch antenna when incorporating optical elements in its radiation path, whereas significant performance degradation of the quasi-Yagi antenna was observed in the previous study [9]. The degradation in the quasi-Yagi antenna is mainly attributed to the large ground plane of the PCB, which affects the function of the partially truncated ground plane of the traditional quasi-Yagi antenna. This effect is not prominent in the patch antenna due to grounding of the entire backside of the patch substrate. Thus, a layer of shielding is provided for circuits integrated on the PCB. Second, the radiation pattern from the patch antenna is more suitable for dual-mode RF/FSO functions than that of quasi-Yagi antenna. The maximum gain direction of the patch antenna is perpendicular to the antenna substrate,

Manuscript received February 14, 2010; revised October 14, 2010; accepted November 11, 2010. Date of publication January 20, 2011; date of current version April 08, 2011. This work was supported in part by a seed grant of Rensselaer Polytechnic Institute (RPI) , in part by the National Science Foundation (NSF) smart lighting ERC at RPI, in part by FRAC award at Tufts University, and in part by University of Massachusetts, the Collaborative Biomedical Research (CBR) Program grant. This work was recommended for publication by Associate Editor A. Shapiro upon evaluation of the reviewers comments.

J. Liao and Z. R. Huang are with the Department of Electrical, Computer and Systems Engineering, Rensselaer Polytechnic Institute, Troy, NY 12180 USA (e-mail: liaoj2@rpi.edu; zrhuang@ecse.rpi.edu).

A. O. Mirvakili and V. M. Joyner are with Department of Electrical and Computer Engineering, Tufts University, Medford, MA 02155 USA (e-mail: ali.mirvakili@tufts.edu; vjoyner@ece.tufts.edu).

A. Boryssenko is with A&E Partnership, Belchertown, MA 01007 USA (e-mail: anatoliy@ae-partnership.com)

Color versions of one or more of the figures in this paper are available online at http://ieeexplore.ieee.org.

Digital Object Identifier 10.1109/TCPMT.2010.2101730

which is more desirable for our application since the optical elements are surface emitting laser diodes. Third, the electric field distribution on the patch and the substrate can be controlled by choosing a proper patch resonance mode. As a case in point, for the fundamental TM_{010} mode, the electric field along the center of the patch is zero for nonradiating patch edges while its maximum for the radiating patch edges associated with a given linear polarization when the patch length is about half wavelength. When the optical device is placed along the center of the nonradiating patch edges, the RF-to-optical coupling should be minimized. In this paper, packaging of optical elements on a modified planar patch antenna to obtain a RF/FSO receiver with enhanced performance is demonstrated. The traditional patch antenna was modified by placing several bonding pads along the center area of the nonradiating patch edges. A bare die p-i-n photodiode(PIN) is placed on the bonding pads and wirebonded to the adjacent optical receiver circuits on the PCB. We analyze the coupling between the RF and the optical link, and verify the simulation results with experimental data. Some measurements of critical importance are compared with the previous study using the quasi Yagi-antenna. As shown in this paper, the coupling from the patch antenna to RF/FSO receiver board is smaller than that from the quasi-Yagi antenna. In addition, the radiation efficiency of the patch antenna is much higher than the quasi-Yagi antenna. In addition, the resonant frequency, polarization, radiation pattern and impedance of patch antenna are easy to adjust [11]. Although patch antennas are inherently narrowband compared to Yagi antennas, the RF cannel bandwidth is not an issue for this study.

II. Design and Fabrication of Modified Patch Antenna

A. Principle of Modified Patch Antenna

A typical patch antenna contains a very thin metal radiator on the top, an insulating substrate in the middle layer, and a large ground plane on the backside of the substrate. The thickness of the dielectric substrate is much smaller than the free-space wavelength at the operation band. There are various substrates that can be used for the fabrication of patch antennas with dielectric constants typically ranging from 2.2 to 12. In this paper, a patch antenna fabricated on two different substrates is investigated. One demonstration employs the RT/Duroid 5880 substrate, which has a dielectric constant of 2.2, and loss tangent of 0.0009 at 10 GHz. The thickness of this substrate is 0.8 mm, and the effective dielectric constant is approximately 2.05. A low dielectric constant is normally desired as it provides larger bandwidth and higher efficiency, but with larger antenna area. The second substrate is the RT/Duroid 6010, which has a dielectric constant of 10.2 and loss tangent of 0.0023 at 10 GHz. The thickness of this substrate is 0.635 mm, and the effective dielectric constant is about 8.70. A large dielectric constant can bring down the overall antenna dimension, which is desirable for the miniaturized RF subsystem and integrated circuits. However, the efficiency and bandwidth of the patch antenna on high dielectric substrate is not as good as antenna on low dielectric substrate [12]. In this paper, the antennas fabricated on RT/Duroid 5880 and RT/Duroid 6010 is referred to as low-K patch antenna and high-K patch antenna, respectively.

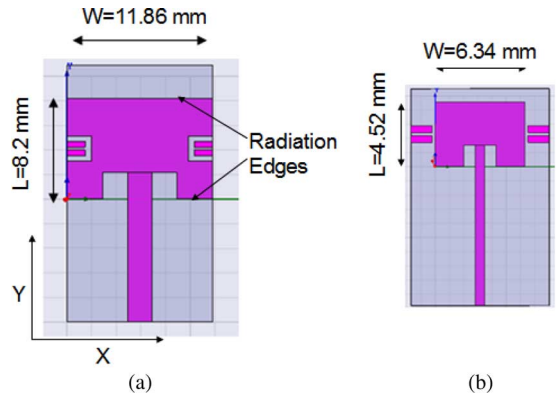

Fig. 1. HFSS model of microstrip patch antenna (a) on low dielectric substrate, (b) on high dielectric substrate.

The modes that can exist in the patch antenna are determined by the patch length (L), patch width (W), and substrate parameters as thickness and dielectric constant. By selecting proper L and W, different modes and field configurations can be achieved. For a rectangular patch, the patch length is normally slightly smaller than half wavelength to get the fundamental mode (TM_{010}), as well as, end-fire radiation pattern. For the TM_{010} mode, the electric field is minimal along the center line of the patch radiator (parallel to the *x* direction in Fig. 1). Therefore, if the optical components are placed at the center where the electric field goes to near zero, a minimized mutual coupling is attainable between the antenna driving port and the collocated optical elements. The radiation edges of the patch antenna are these two fringing field parts, as shown in Fig. 1(a).

There are two major differences between the modified patch antenna and the traditional rectangular patch antenna. One difference is that the substrate of the modified patch antenna is truncated as shown in Fig. 1. Normally, the patch substrate dimension is much larger than the patch metal radiator so that the ground plane and the substrate can be assumed infinitely large in the XY plane. However, the substrate dimension of the antenna in the RF/FSO receiver board is limited by the requirements for optical device assembly and wire bonding. Therefore, the patch antenna substrate is truncated in both X and Y direction. In this case, the infinite substrate and ground plane assumption in traditional patch antenna analysis is no longer valid. Besides, the fringing field distribution is also distorted. Therefore, the patch length and width in the RF/FSO receiver board are different from that for the traditional patch antenna at the same operation frequency. The second difference is the optical bonding pads. As the presence of the bonding pads along the center of the patch, the return loss and radiation pattern will also be distorted. These factors will be explained in detail in Sections II-B and II-C.

B. Design of Modified Patch Antenna

We designed the patch antenna following the general design guidelines [12]. As the dimensions of the patch are finite along X and Y direction, the fields at the edges of the patch will undergo fringing. Moreover, the fringing field is a function of the patch length, the substrate thickness and the dielectric constant. Consequently, an effective length is used in the patch antenna

design to include the fringing effect. With the consideration of fringing field, the actual patch length is

$$L = \frac{\lambda}{2} - 2\Delta L = \frac{\lambda}{2} - 2 \times h \times 0.412 \frac{(\varepsilon_{\text{reff}} + 0.3)\left(\frac{W}{h} + 0.264\right)}{(\varepsilon_{\text{reff}} - 0.258)\left(\frac{W}{h} + 0.8\right)} \quad (1)$$

where W is the patch width, h is the substrate thickness, $\varepsilon_{\text{reff}}$ is the effective substrate dielectric constant, and λ is the wavelength in the substrate.

For an efficient patch radiator [12], the width W should be

$$W = \frac{v_o}{2 \times f} \sqrt{\frac{2}{\varepsilon_r + 1}} \quad (2)$$

where v_0 is speed of light in free space, f is the resonant frequency, and ε_{r} is the substrate dielectric constant.

There are different methods for feeding the RF signal into the patch antenna, such as microstrip line feed, probe feed, aperture-coupled, proximity-coupled feed. [12]. Among these methods, the microstrip line feed is easy to fabricate, simple for impedance matching and desirable for integrated circuit fabrication. However, it may cause bandwidth narrowing and generation of higher order modes around the feed line edges. The microstrip line feed was chosen for this study. To avoid the higher order modes, the width and length of the recessed microstrip line are optimized by Ansoft HFSS.

From (1) and (2), an approximate value of W and L is derived. For the low-K patch antenna, $\mathrm{W} = 11.54$ mm and $\mathrm{L} = 9.65$ mm. For the high-K patch antenna, $\mathrm{W} = 6.24$ mm and $\mathrm{L} = 4.4$ mm. However, due to the truncation of the substrate and the presence of the optical bonding pads, the calculated results from the above equations can only be used as a starting point for the optimized antenna design. Besides, the metal-removed gaps slots around the bonding pads and the recessed microstrip feed impedance match gaps excite higher order modes. To accommodate the antenna radiation degradation due to the above-mentioned reasons, the dimension of the bonding pads and the recessed microstrip feed slot is optimized using HFSS software. For the bonding pads and the slots between these pads, the dimension should be as small as possible to minimize the coupling from the antenna to optical link. This is because, with smaller bonding pads, the optical devices and bonding wires are closer to the center of the patch where the electric field is zero. Besides, smaller bonding pads and slots have less perturbation to the antenna radiation pattern and also less return loss. With the consideration of optical device dimension and wire bonding requirements, the final bonding pad's dimension is determined as 1.5 mm×0.5 mm. Moreover, the gaps width between the bonding pads is 0.2 mm. For the recessed microstrip feed part, the recession length is adjusted to achieve 50-Ω impedance match, and the metal gap in X direction is adjusted by HFSS to suppress higher order modes. With the fine optimization using HFSS, the antenna dimension is determined as follows: for the low-K patch antenna, $\mathrm{W} = 11.86$ mm, and $\mathrm{L} = 8.2$ mm; for the high-K patch antenna, $\mathrm{W} = 6.34$ mm, and $\mathrm{L} = 4.52$ mm. Both operate being tuned to the targeted frequency 10 GHz.

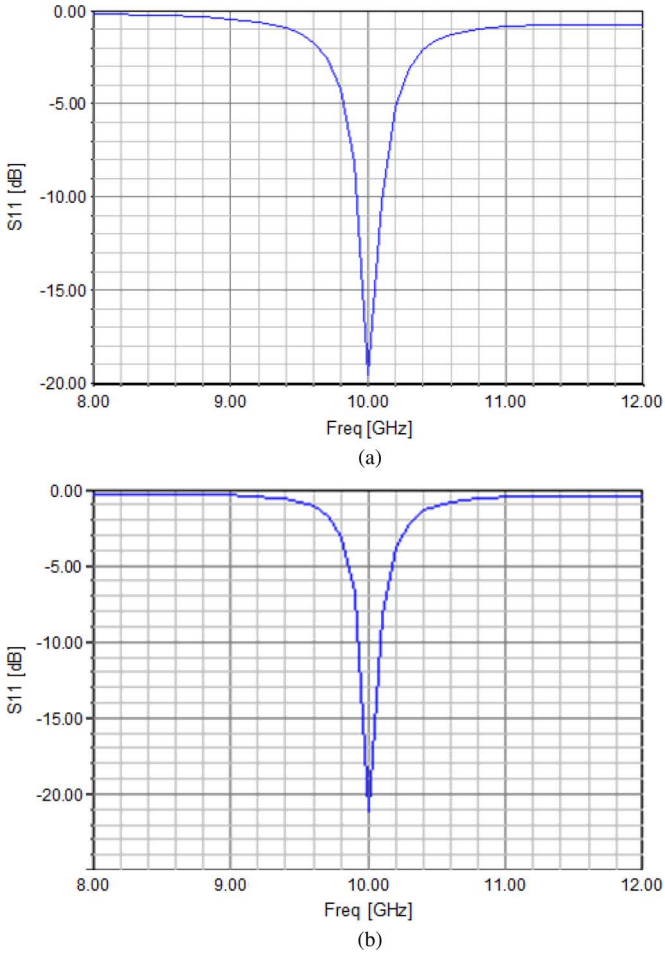

Fig. 2. The return loss of the patch antenna on (a) low-K dielectric substrate and (b) high-K dielectric substrate.

C. Simulation Results

Using the antenna dimension determined above, the return loss and radiation pattern for both low-K and high-K antennas are computed by HSFF and shown in Figs. 2 and 3, respectively. According to Fig. 2, the −10 dB S11 bandwidth is about 0.18 GHz for the low-K patch antenna and 0.15 GHz for the high-K patch antenna. Hence, the bandwidth of patch antenna is much smaller than the bandwidth (1.4 GHz) of the quasi-Yagi antenna [9].

As indicated by Fig. 3, both antennas exhibit end-fire radiation patterns. The z-direction gain is 5.16 dBi for the low-K patch antenna, and 3.54 dBi for the gain of high-K patch antenna. In previous study, the realized gain of quasi-Yagi antenna was 0.5 dBi [9], which is much smaller than the gain of the patch antenna.

D. Fabrication of the Modified Patch Antenna

Both antennas are fabricated in a standard class 100 clean room. The antenna structures are first drawn by CAD tools, and

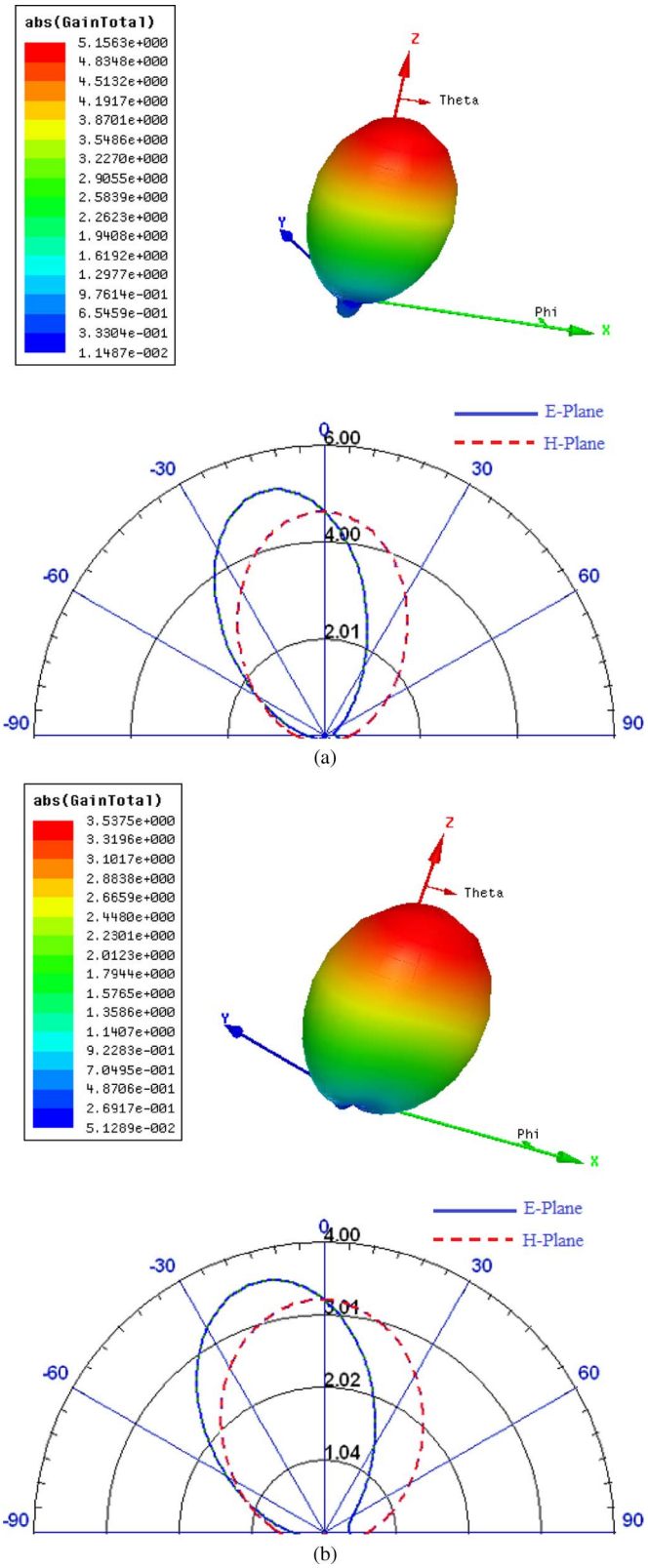

Fig. 3. Radiation pattern of the patch antenna on (a) low dielectric substrate and (b) high dielectric substrate.

printed on transparent masks. Then the antenna pattern is transferred to the Duroid board by photolithography and development. PCB etching solution is used to etch the unwanted copper. The photo of a fabricated patch antenna on low ε dielectric substrate is shown in Fig. 4.

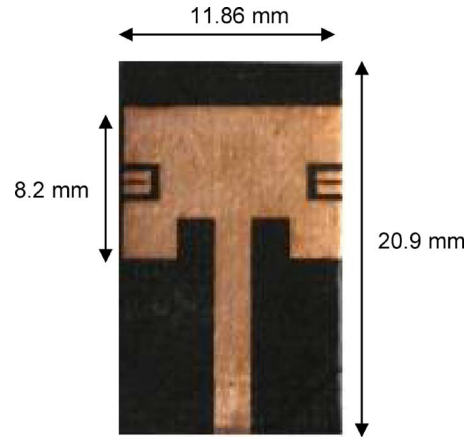

Fig. 4. Photograph of a fabricated patch antenna.

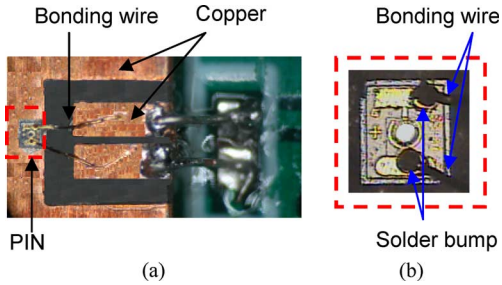

Fig. 5. (a) Packaging of PIN to RF/FSO receiver board. (b) Bonding wires on PIN.

III. Packaging of PIN on Patch Antenna For RF/FSO Receiver

As indicated in previous study [8], the coupling from antenna to transmitter is negligible. The antenna-induced current on the receiver board is the dominate noise source for the FSO link. Therefore, in this paper, we mainly focused on investigation of the cross channel coupling on a RF/FSO receiver board. A commercial high speed optical transmitter (F425S17485 Small Form Factor Pluggable transceiver module) and a PIN are used to construct the end-to-end FSO link. In the optical receiver end, a bare die top-illuminated GaAs PIN (PDCS70T-GS from Enablence) is employed to detect the modulated optical signal. The dimension of the PIN die is $350 \times 300 \times 150\ \mu\text{m}^3$, and the diameter of the active area is 70 μm. Both the p-contact and n-contact are on the top surface. The PIN is attached to the antenna by epoxy adhesive (Resinlab SEC 1233). The epoxy is silver filled with two components: base resin and catalyst, which are mixed with 1:1 ratio in room temperature. A small droplet, $\sim 200\ \mu$m in diameter, is placed on the antenna near the bonding pads for the attachment of optical elements. The PIN is placed on the epoxy drop, and then cured in an oven at 60 °C for 1 h. Then, the p-contact of the PIN is bonded to the upper bonding pad by a 1-mil gold wire, as shown in Fig. 5, and the n-contact is bonded to the lower bonding pad.

The patch antenna with the assembled PIN is attached to a multilayer FR4 PCB using epoxy adhesive (Loctite Hysol 608), on which the transimpedance amplifier (TIA) circuits are integrated. The TIA (MAX3864) is used to amplify the single-ended photocurrent signal from the PIN to a differential output voltage

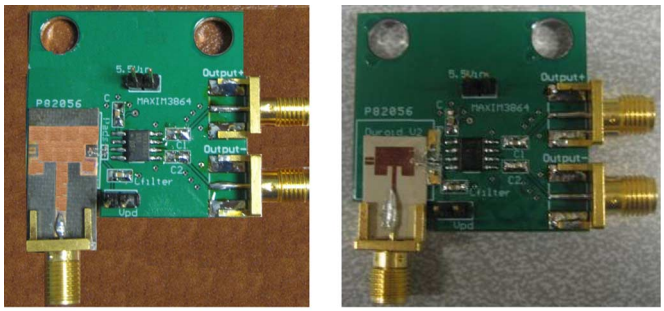

(a) (b)

Fig. 6. Photograph of RF/FSO receiver board built with (a) patch antenna on low dielectric substrate, (b) patch antenna on high dielectric substrate.

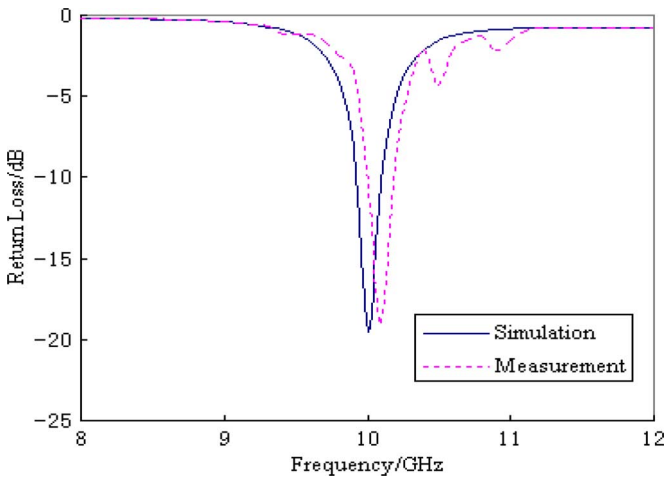

Fig. 7. Simulated and measured return loss for the low-K patch antenna.

for measurement. This TIA with a single 5.0 V supply voltage and 0.85 pF source capacitance, which represents the total input capacitance, achieves a bandwidth of 2 GHz and dynamic range of −24 dBm to 0 dBm. In addition, this TIA with the input-referred rms noise of 490 nA can operate up to 2.5 Gb/s. The differential outputs of the TIA are ac coupled to 50-Ω transmission lines and routed to edge-connected SMA connectors. The RF/FSO receiver boards for both low-K and high-K antenna are shown in Fig. 6.

For the RF channel, the patch antenna can be used to transmit and receive electromagnetic wave that carries information signal. RF driver or amplifier circuit design is not included in this paper. Indeed, we used a SMA connector to get direct communication between antenna and RF measurement equipments.

IV. Analysis and Measurement of RF Channel

A. Patch Antenna Return Loss Measurement

The return loss of the antenna is measured by a network analyzer (Agilent 8510 C). The blue solid curve in Figs. 7 and 8 show the simulated return loss of the antennas, and the red dash curve is the measurement result. As shown in these figures, the patch antenna demonstrates low return loss at 10 GHz. The measurement result differs slightly from the simulation curve, which is attributed to impedance mismatch introduced by the solder joints around SMA connector. We also observed that the high-K

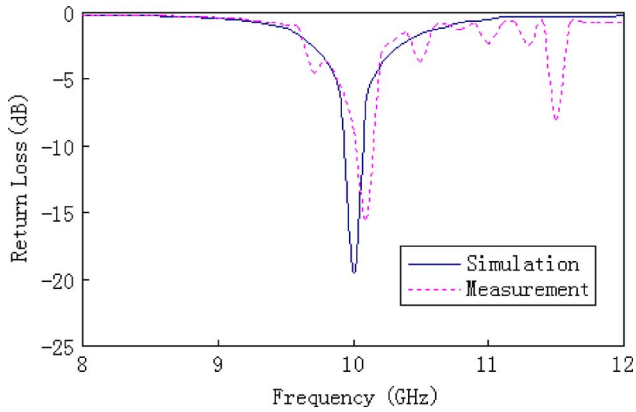

Fig. 8. Simulated and measured return loss for the high-K patch antenna.

patch antenna has smaller bandwidth than low-K patch antenna. Accordingly, both antennas have inherently narrower bandwidth than the quasi-Yagi antenna [8]–[10] as early mentioned.

It is a quite typical discrepancy observed in Fig. 7 between the simulated and measured S_{11} curve. It happens because the microstrip patch antenna is a high-Q resonance device sensitive to tolerances and numerical errors. At practice, the antenna might be tuned to a particular operational frequency by making its second design iteration. In our case of feasibility studies, it is possible to tune the antenna to a particular frequency to perform the tests at that frequency close to the projected one. Also, it is worth to note that the achieved level of impedance matching around −20 dB of return loss is very good for the measurement.

The discrepancies observed in Fig. 8 can explained in a similar fashion as for the case on low-K substrate. Additionally, the ripples of S_{11} possibly originate due to substrate truncation for the higher value of dielectric constant. In the future, the model of SMA connector can be included in the simulation to account for its impact on the antenna performance.

B. Patch Antenna Radiation Pattern Measurement

The near field radiation pattern of both low-K and high-K patch antenna is measured in an anechoic chamber using equipment from Nearfield Systems Inc. (NSI, Torrance, CA). The measured near field radiation pattern is then converted to far field pattern by Fourier transform. Since the cross-polarization component is significantly smaller than the co-polarization component, only the co-polarization far field radiation pattern is shown in Figs. 9 and 10. Fig. 9 shows the radiation pattern for the low-K patch antenna. In Fig. 9(a), the radiation when optical receiver is powered on is shown. Based on this figure, the H plane field is close to a typical patch antenna radiation pattern. However, The E plane field is distorted, and the maximum gain appears at 45° direction. This is because the Duroid substrate to the left of the patch board is truncated, and circuit elements are placed on the right side of the patch antenna. These perturbations in the electromagnetic environment distort the ideal radiation pattern. However, as the alignment of the RF link is not critical, and the antenna can cover a large field-of-view, the distortion in the antenna radiation pattern will not degrade RF link performance too much. In Fig. 9(b), the radiation pattern for the same antenna when optical receiver is powered off is

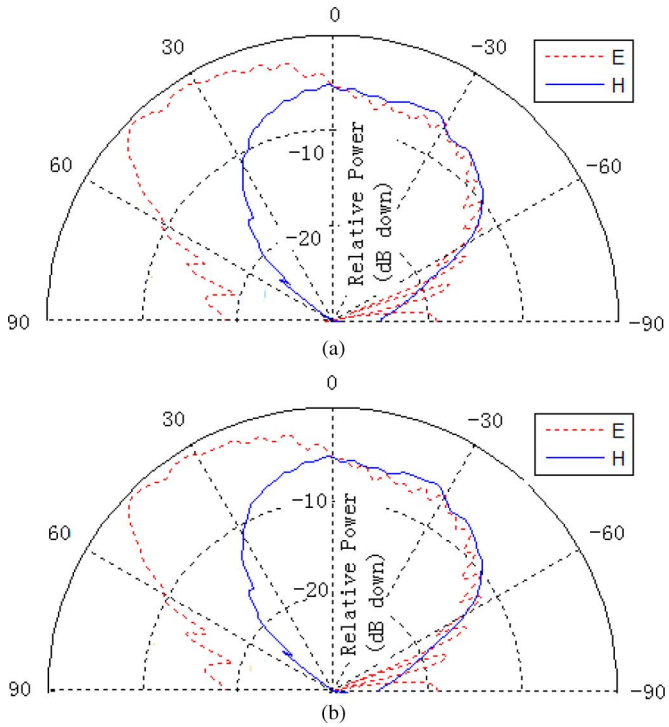

Fig. 9. Radiation pattern of the low-K patch antenna at 10 GHz: (a) receiver powered on, (b) receiver powered off.

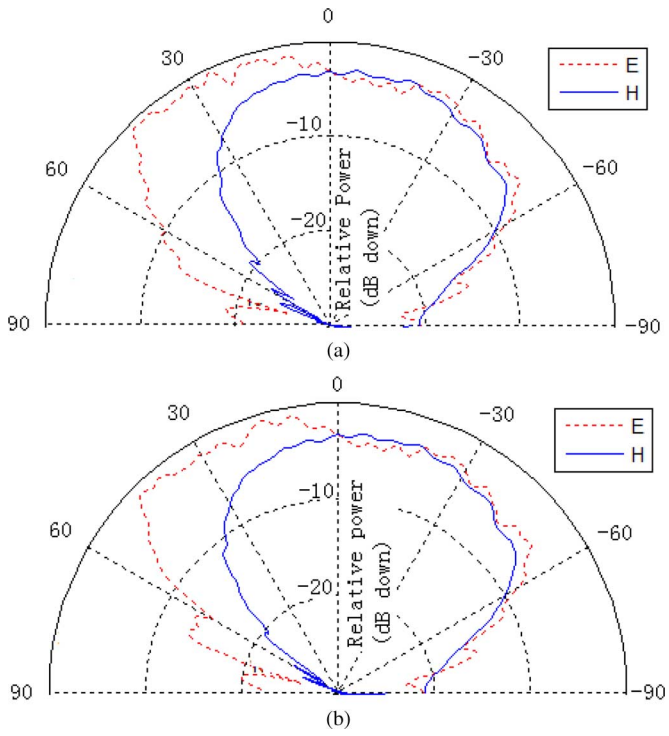

Fig. 10. Radiation pattern of the high-K patch antenna at 10 GHz: (a) receiver powered on, (b) receiver powered off.

shown. No noticeable difference between Fig. 9(a) and (b) is observed. Therefore, the optical receiver has negligible effect on the antenna radiation pattern in regard of sensitivity of radiation pattern measurement.

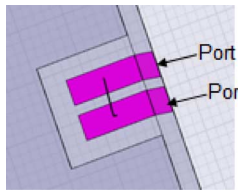

Fig. 11. HFSS model for RF/FSO coupling analysis.

In Fig. 10, the radiation pattern of the high-K patch antenna is shown. Similar to the low-K patch antenna, the maximum gain direction of E plane radiation is shifted. However, the distortion of the high-K antenna radiation pattern is not as severe as that of the low-K patch antenna. The main reason is that there is a 1.7-mm-wide Duroid substrate to the left of the high-K patch antenna, as shown in Fig. 1(b). The radiation pattern is measured when the optical receiver is powered on and off. Results are shown in Fig. 10(a) and (b), respectively. As shown in these figures, no significant difference between these two cases is observed.

V. RF To FSO Link Coupling Analysis

A. Simulation of the Coupling From RF to Optical Link

In the RF/FSO dual mode transceiver board, as the optical device and associated circuitry share common structural components with the patch antenna, electromagnetic coupling is present between the RF and FSO components. This coupling might affect the signal-to-noise ratio, and thus degrade the system's performance. To study the coupling effect, HFSS software was used to model the energy leakage from RF port to FSO port as depicted in Fig. 11. The optical ports are assigned near the optical device bonding pads, and each port has a characteristics impedance of 50 Ω. Gold bonding wires with length of $\sim 765\ \mu$m connect the two pads. The optical ports, bonding pads and bonding wire represent the optical front-end that will interact with the patch antenna.

The computed magnitude of EM coupling for both low-K and high-K patch antenna, which is observed between the antenna port (port 1) and two optical ports (port 2 and 3), is plotted in Figs. 12 and 13 with respect to the 50-Ω reference impedance, respectively. For the low-K patch antenna, the coupling approaches the magnitude of smaller than 26 dB in the antenna's operational band around 10 GHz. For the high-K patch antenna, the coupling from RF to FSO is smaller than 16 dB. For both antennas, the dimension of the bonding pads and bonding wire are identical. However, because of the smaller dimension of high-K patch antenna, the bonding pads are not exactly along the center line of the patch radiator (parallel to the x direction in Fig. 1) and produce large disturbance for the resonance field. Consequently, there will be more coupling from RF-to-optical link in the high-K patch antenna RF/FSO system.

B. Measurement of the Coupling From RF to Optical Link

To test the RF/FSO receiver, a free space link on the optical table is constructed, as shown in Fig. 13. In this setup, the commercial transceiver module, which is driven by the Anritsu

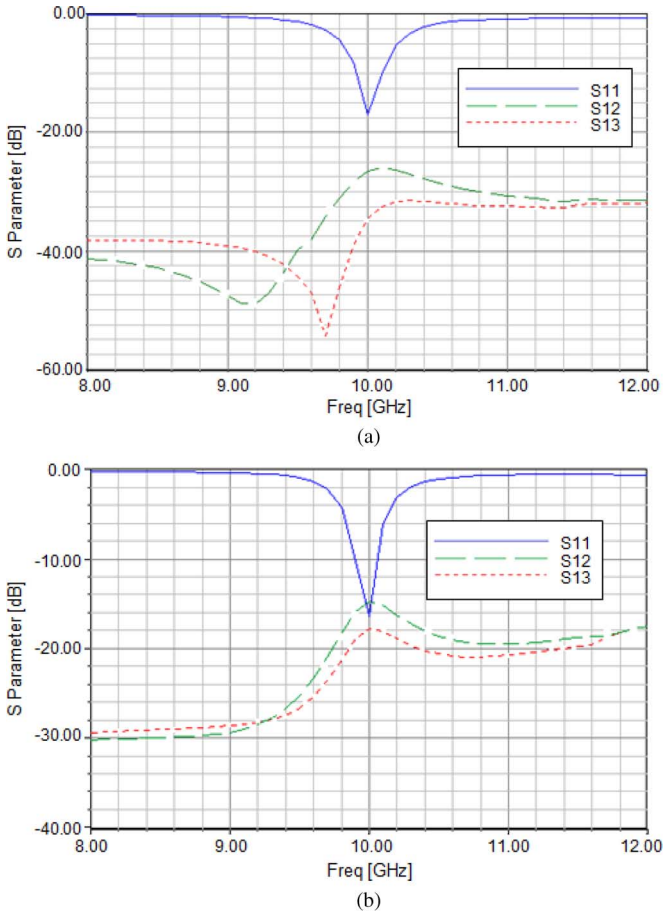

Fig. 12. Coupling from RF to FSO link for (a) low-K patch antenna; (b) high-K patch antenna.

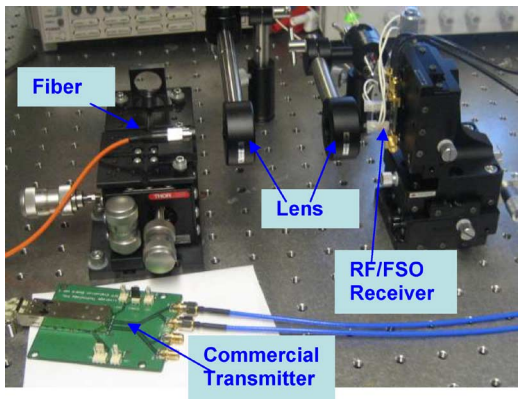

Fig. 13. Experimental setup for the FSO link measurement.

MP1800A pulse pattern generator (PPG), is used to transmit modulated optical signals. The PPG provides a differential 2 Gb/s $2^{31} - 1$ nonreturn-to-zero (NRZ) pseudorandom binary sequence (PRBS). The laser beam is coupled into a multimode fiber, which is mounted on a precision three dimensional translation stage. Two lenses are used for beam alignment. Lens 1 is used to collimate the output beam from the multimode fiber, and Lens 2 focuses the collimated beam onto the photodiode active area. The receiver board is connected to a digital sampling

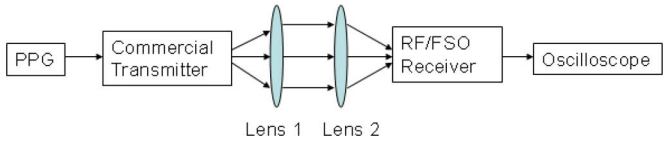

Fig. 14. Schematics of the FSO link test setup.

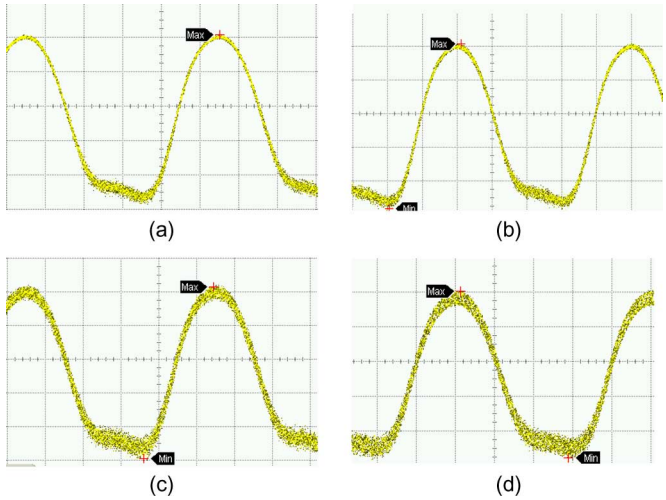

Fig. 15. Measured transient output waveform at 2 Gb/s for the low-K patch antenna prototype board when the RF antenna port is fed with different power levels: (a) no RF signal; (b) 0 dBm; (c) 7 dBm; (d) 14 dBm.

oscilloscope (Agilent DCA-J 86100C) to observe the received waveform. The experimental setup is shown in Fig. 14 and the distance between the transmitter and the receiver is about 10 cm. The biggest challenge for the FSO link measurements is the beam alignment as the active area of the bare die photodiode is small ($\sim$ 70 μm). To receive maximum optical power, the relative position of the multimode fiber and Lens 1 is fine tuned to ensure that the output beam is collimated. Then, the position of Lens 2 and the receiver board is adjusted in x-, y-, and z-axes to find the maximum photocurrent.

To determine the relationship between the antenna power level and the EM coupled noise level, four different RF power levels (0, 0 dBm, 7 dBm, and 14 dBm) are studied. An Agilent E8257D signal generator is used to feed CW RF power at 10 GHz into the patch antenna. Fig. 15 shows the transient output waveforms for the low-K patch antenna receiver board. Comparing Fig. 15(a)–(d), it is observed that the noise level is about 3.9 mV. The total peak-to-peak signal amplitude is 248 mV.

Fig. 16 shows the eye pattern for the low-K patch antenna receiver board when the RF antenna port is fed with different power levels. Since the noise is much smaller than the signal level, the degradation of the eye diagram is not prominent.

For the RF/FSO receiver boards built with high-K patch antenna, we used the same setup to test transient output and eye diagram. Fig. 17 shows the transient output waveform for the high-K patch antenna's receiver board. As shown in these figures, the noise level is about 6.1 mV, which is much smaller than signal level (197 mV).

Fig. 18 shows the eye pattern for the high-K patch antenna receiver board when the RF antenna port is fed with different

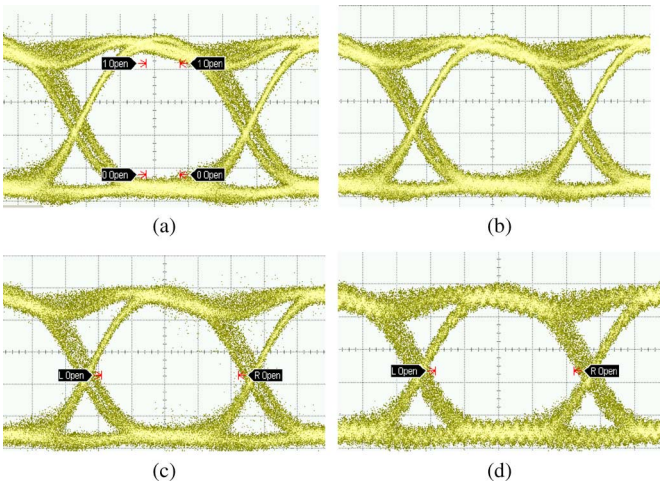

Fig. 16. Measured 2 Gb/s eye pattern for the low-K patch antenna prototype board when the RF antenna port is fed with different power levels: (a) no RF signal; (b) 0 dBm; (c) 7 dBm; (d) 14 dBm.

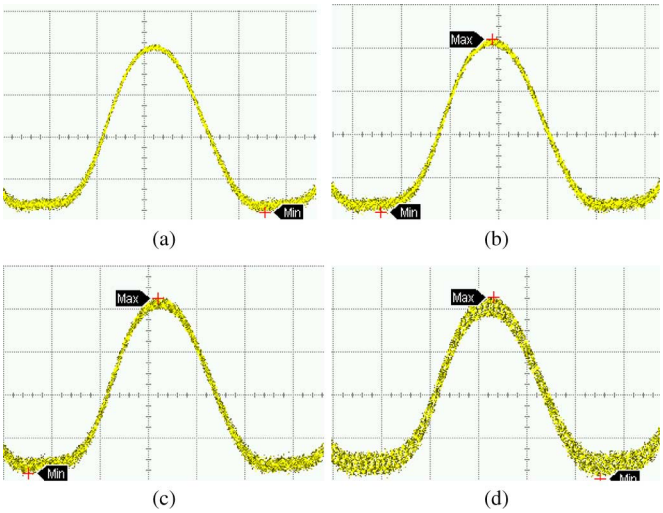

Fig. 17. Measured transient output waveform at 2 Gb/s for the high-K patch antenna prototype board when the RF antenna port is fed with different power levels: (a) no RF signal; (b) 0 dBm; (c) 7 dBm; (d) 14 dBm.

power levels. There is no significant degradation in the eye diagram with different RF fed powers

From the previous study, the coupling level in the RF/FSO system built upon quasi-Yagi antenna is 14.8 mV [8], [9]. To compare the RF/FSO system performance with different antenna prototypes, the critical properties for each antenna are listed in Table I. As the length of the substrate Duroid board is affected by the transmission line and PCB board design, it is not compared here. From the table, the low-K patch antenna has the highest gain and the lowest RF-to-optical coupling. The high-K patch antenna has the smallest antenna dimension. With the optimized patch design, the degradation in the optical receiver end is significantly reduced.

VI. Conclusion

In this paper, we prototyped a new RF/FSO receiver board that incorporates a patch antenna. We modified the conventional

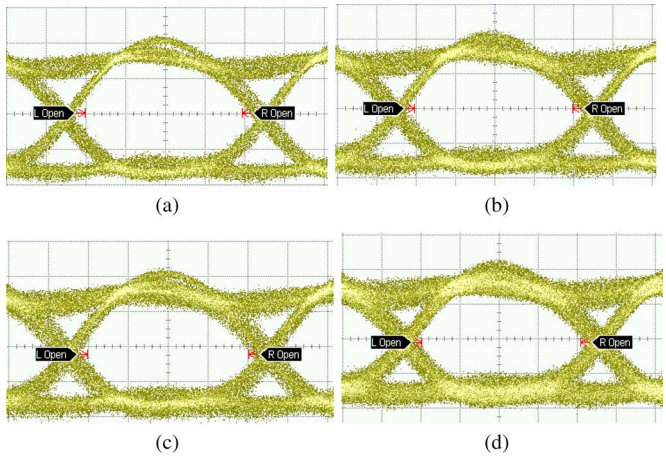

Fig. 18. Measured eye pattern at 2 Gb/s for the high K patch antenna prototype board when the RF antenna port is fed with different power levels: (a) no RF signal; (b) 0 dBm; (c) 7 dBm; (d) 14 dBm.

TABLE I
Comparison of RF/FSO Receiver Module on Quasi-Yagi Antenna, High-K Patch and Low-K Patch Antenna

Antenna type	Quasi-Yagi Antenna	High-K patch	Low-K patch
Antenna gain(dBi)	0.5	3.54	5.16
Antenna to FSO coupling (mV)	14.8	6.1	3.9
Antenna width(mm)	13	9.74	11.86

patch antenna by adding optical bonding pads in the center of the patch nonradiating edge. Both simulation and experimental results show that this new system is more robust compared to previously investigated RF/FSO system on quasi-Yagi antenna. The antenna gain has increased from 0.5 to 5.16 dBi., the antenna dimension has reduced, and the antenna to optical link coupling was reduced from 14.8 to 3.9 mV. Patch antennas on both low and high dielectric substrates are investigated to accommodate different applications. FSO link transmission at 2 Gb/s in a 10 GHz RF environment is achieved with negligible interference.

References

[1] J. M. Kahn and J. R. Barry, "Wireless infrared communication," *Proc. IEEE*, vol. 85, no. 2, pp. 265–298, Feb. 1997.
[2] T. Rokkas, T. Kamalakis, D. Katsianis, D. Varoutas, and T. Sphicopoulos, "Business prospects of wide-scale deployment of free space optical technology as a last-mile solution: A techno-economic evaluation," *J. Opt. Network.*, vol. 6, no. 7, pp. 860–870, Jul. 2007.
[3] E. Leitgeb, M. Gebhart, U. Birnbacher, W. Kogler, and P. Schrotter, "High availability of hybrid wireless network," in *Proc. SPIE*, Strasbourg, France, Apr. 2004, vol. 5465, pp. 238–249.
[4] H. Izadpanah, T. ElBatt, V. Kukshya, F. Dolezal, and B. K. Ryu, "High-availability free space optical and RF hybrid wireless networks," *IEEE Wireless Commun.*, vol. 10, no. 2, pp. 45–53, Apr. 2003.
[5] S. D. Milner and C. C. Davis, "Hybrid free space optical/RF networks for tactical operations," in *IEEE Military Commun. Conf.*, Oct.–Nov. 2004, vol. 1, pp. 409–415.
[6] B. W. Cook, S. Lanzisera, and K. S. J. Pister, "SoC issues for RF smart dust," *Proce. IEEE*, vol. 94, no. 6, pp. 1177–1196, Jun. 2006.
[7] J. J. Lin, L. Gao, A. Sugavanam, X. Guo, R. Li, J. E. Brewerand, and K. K. O. , "Integrated antennas on silicon substrates for communication over free space," *IEEE Electron Device Lett.*, vol. 25, no. 4, pp. 196–198, Apr. 2004.

[8] J. Liao, J. Zeng, S. Deng, V. Joyner, A. Boryssenko, K. Connor, and Z. R. Huang, "Packaging of optoelectronic and RF components with shared elements for dual-mode wireless communications," *Electron. Lett.*, vol. 45, no. 8, pp. 411–412, Apr. 2009.

[9] A. Boryssenko, J. Liao, J. Zeng, V. Joyner, and Z. R. Huang, "Studies on RF-optical dual mode wireless communication modules," in *IEEE Microwave Theory Tech. Soc. Int. Microwave Symp.*, Jun. 2009, pp. 805–808.

[10] J. Liao, S. Deng, F. Smith, Z. R. Huang, and K. Connor, "Integrated laser diodes and photodetectors with antenna for dual-mode wireless communication," in *Proc. 20th Annu. Meeting IEEE Lasers Electro-Optics Soc.*, Oct. 2007, pp. 264–265.

[11] C. A. Balanis, *Antenna Theory: Analysis and Design*, 2nd ed. New York: Wiley, 1997.

[12] S. J. Orfanidis, Electromagnetic waves and antennas ch. 18 [Online]. Available: http://www.ece.rutgers.edu/~orfanidi/ewa/ch18.pdf

Jun Liao (M'07) received the B.S. degree from Beijing University of Posts and Telecommunications, Beijing, China in 2006. He is currently pursuing the Ph.D. degree in the Department of Electrical, Computer and Systems Engineering, Rensselaer Polytechnic Institute, Troy, NY.

His research interest includes RF/opto hybrid packing, planar antenna design and free space optical communication.

Ali Mirvakili (M'09) received the B.S. degree from Yazd University, Yazd, Iran, in 2005, and the M.S. degree from K. N. Toosi University of Technology, Tehran, Iran, in 2008, both in electrical engineering, He is currently working towards the Ph.D. degree in the Department of Electrical eEngineering at Tufts University, Medford, MA.

His research interest includes VLSI (analog, digital and mixed-signal circuits) and CMOS integrated circuit design for high-speed optical and RF wireless applications.

Anatoliy O. Boryssenko received the M.Sc. E.E. and Ph.D. E.E. degrees from the Kiev Polytechnic Institute, Kiev, Ukraine.

He worked as an Associate Professor of the Kiev Polytechnic Institute and as an R&D engineer in companies related to millimeter-wave and UWB communication and sensor systems. His research interests include subsurface radar imaging; broadband and UWB antenna and array design; applied and computational electromagnetics; signal processing and system design for radar, sensing and imaging. Since 2000, he has worked for the University of Massachusetts, Amherst. Now he is a Research Associate Professor of the Electrical and Computer Engineering Department. Now he is with A&E Partnership, Belchertown, MA.

Valencia M. Joyner (M'98) received the S.B. and M.Eng. degrees in electrical engineering and computer science from the Massachusetts Institute of Technology, Cambridge, in 1998 and 1999, respectively, and the Ph.D. degree from the University of Cambridge, Cambridge, U.K., in 2003.

She is currently an Assistant Professor at Tufts University in Medford, MA, where she leads the Advanced Integrated Circuits and Systems Group. Her current research interests include opto-electronic integrated circuit design for high-speed optical and RF wireless networks and biomedical imaging applications.

Dr. Joyner was awarded a Marshall Scholarship and NSF Graduate Research Fellowship.

Zhaoran Rena Huang (M'99) received the B.S. degree from Beijing Institute of Technology, Beijing, China, in 1995, and the M.Sc. and Ph.D. degrees from Georgia Institute of Technology, Atlanta, in 1999 and 2003, respectively.

She is currently an Assistant Professor at Rensselaer Polytechnic Institute, Troy, New York. Her current research focus includes RF/opto packaging for high-speed low power wireless communication, and integrated photonics for next-generation lightwave technology.